

Chemical Science

Accepted Manuscript



This is an *Accepted Manuscript*, which has been through the Royal Society of Chemistry peer review process and has been accepted for publication.

Accepted Manuscripts are published online shortly after acceptance, before technical editing, formatting and proof reading. Using this free service, authors can make their results available to the community, in citable form, before we publish the edited article. We will replace this *Accepted Manuscript* with the edited and formatted *Advance Article* as soon as it is available.

You can find more information about *Accepted Manuscripts* in the [Information for Authors](#).

Please note that technical editing may introduce minor changes to the text and/or graphics, which may alter content. The journal's standard [Terms & Conditions](#) and the [Ethical guidelines](#) still apply. In no event shall the Royal Society of Chemistry be held responsible for any errors or omissions in this *Accepted Manuscript* or any consequences arising from the use of any information it contains.



www.rsc.org/chemicalscience

EDGE ARTICLE

NMR Characterization of Cooperativity: Fast Ligand Binding Coupled to Slow Protein Dimerization

Cite this: DOI: 10.1039/x0xx00000x

Zil E Huma^a, Justin P. Ludeman^a, Brendan L. Wilkinson^b, Richard J. Payne^c, Martin J. Stone^{a*}Received 00th January 2012,
Accepted 00th January 2012

DOI: 10.1039/x0xx00000x

www.rsc.org/

We describe a general approach for analysis of 2D NMR spectra to evaluate the cooperativity of ligand binding and protein dimerization in coupled systems. The approach is applicable to systems in which NMR spectra display separate resonances for monomeric and dimeric species but each resonance shifts in response to ligand binding. Three experimental parameters (monomer chemical shift, dimer chemical shift and relative monomer:dimer peak intensity) are fitted globally, as a function of ligand concentration, to yield equilibrium constants for dimerization, monomer:ligand binding and dimer:ligand binding as well as the cooperativity between ligand binding and dimerization. We have applied the approach to characterise a system in which dimerization of the chemokine monocyte chemoattractant protein-1 (MCP-1/CCL2) is coupled to binding of peptides derived from the chemokine receptor CCR2. The global fitting approach allowed evaluation of cooperativity with higher precision than is possible by alternative methods.

Introduction

Dimerization is a common property of proteins and frequently influences interactions with binding partners, including proteins, nucleic acids, polysaccharides, lipid membranes, metal ions and small molecules.^{1,2} A fundamental thermodynamic characteristic of such proteins is cooperativity between protein dimerization and ligand binding, defined as the factor by which dimerization enhances (or reduces) the ligand binding affinity. The classical approach to characterize the cooperativity in such coupled systems is to analyze the influence of ligand concentration on the position of the monomer-dimer equilibrium and/or the influence of the total protein concentration on the apparent ligand binding affinity.³⁻⁹ This typically requires an extensive series of experiments; the analysis is further complicated if both monomeric and dimeric species bind to the ligand. In such coupled systems it would be advantageous to measure ligand binding using a technique that simultaneously reports on the dimerization state of the protein. Herein, we show that 2D NMR can achieve this because different features of NMR spectra are sensitive to ligand binding and dimerization. We present a novel theoretical framework for analysis of such 2D NMR data and we demonstrate application of this approach to characterizing the interactions of a chemokine with fragments of a chemokine receptor.

Chemokines are soluble proteins that activate G protein-coupled receptors in leukocyte membranes, thereby inducing leukocyte trafficking in both inflammation and normal immune surveillance.¹⁰⁻¹¹ Most chemokine receptors contain sulfated tyrosine

residues in their extracellular N-terminal regions, the site of initial binding by chemokine ligands, and receptor tyrosine sulfation enhances chemokine binding affinity.^{12,13} Many chemokines dimerize weakly, although members of the two major chemokine families (CC and CXC) have distinct dimer structures.^{13,17} Although the monomeric form is sufficient for receptor binding and activation, the dimeric forms of some CC and CXC chemokines are also able to bind to the N-terminal regions of their receptors^{12,18,19}; the dimeric forms of certain CXC chemokines can even activate their receptors.²⁰⁻²⁴ Here, we analyze the interactions of sulfated N-terminal peptides derived from the chemokine receptor CCR2 with both monomeric and dimeric forms of the chemokine monocyte chemoattractant protein-1 (MCP-1/CCL2).

Results and Discussion

NMR Observation of Coupled Equilibria

Wild type human MCP-1 has been shown previously to dimerize with a dissociation equilibrium constant (K_{MD}) in the low micromolar range.¹⁴⁻¹⁶ The 2D ¹⁵N-¹H NMR spectrum (¹⁵N-HSQC) of MCP-1 displays peaks corresponding to both monomeric and dimeric species, indicating that the rate of exchange between these two forms is slow in comparison to the minimum frequency difference between corresponding monomer and dimer peaks, i.e. slower than ~ 100 s⁻¹. Upon addition of sulfated N-terminal peptides derived from chemokine receptor CCR2, we observe that both monomer and

dimer peaks in the ^{15}N -HSQC of MCP-1 shift monotonically until saturation is reached but they remain as separate resonances (Figures 1 and S1).

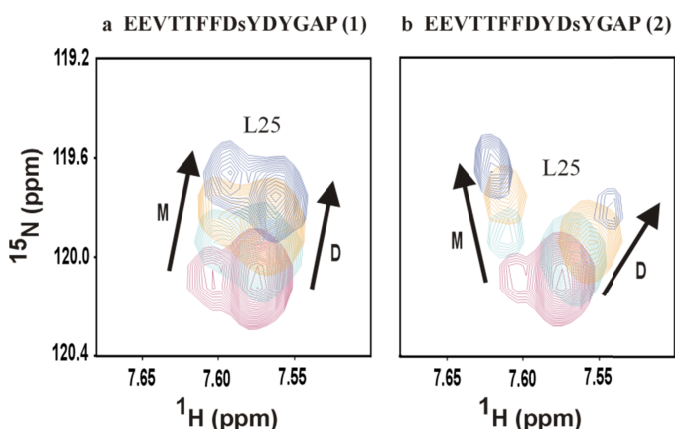


Figure 1. Binding of MCP-1 to sulfopeptides corresponding to a fragment of the CCR2 extracellular domain [CCR2 (18-31)]. A detailed region (Leu-25 NH resonances) of the ^{15}N -HSQC spectrum is shown for 50 μM MCP-1 alone (red) and in the presence of 20 μM (cyan), 50 μM (orange) and 150 μM (blue) of CCR2 sulfopeptides: (a) **1** and (b) **2**, whose amino acid sequences are shown at the top (sY = sulfotyrosine); the sulfopeptides have free N-termini and C-terminal amide moieties. Sulfopeptide-induced shifts of monomer (M) and dimer (D) resonances are indicated by arrows.

This indicates that (1) both the monomeric and dimeric species are binding to the peptide; (2) the rate of exchange between the free and bound forms of the monomer (or of the dimer) is fast in comparison to the frequency differences between free and bound resonances (faster than $\sim 100\text{ s}^{-1}$); and (3) the rate of exchange between the bound monomer and bound dimer species remains slow in comparison to the monomer-dimer frequency differences. However, in addition to undergoing frequency changes in response to ligand binding, the relative intensities of the monomer and dimer peaks also change, indicating that ligand binding alters the position of the monomer-dimer equilibrium. Thus, the spectra contain independent parameters [change in monomer chemical shift (m); change in dimer chemical shift (d); and the ratio of monomer to dimer peak intensity (r_{MD})] that report on each of the three equilibrium processes [monomer:peptide binding; dimer:peptide binding; and monomer-dimer equilibrium, respectively]. In theory, these three parameters can be used to fully characterize the thermodynamics of the coupled equilibrium system, including cooperativity.

Thermodynamic Model of Coupled Equilibria

The simplest thermodynamic model to explain these data is the set of coupled equilibria shown in Figure 2. This model contains five equilibrium constants of which only three are independent (coloured red in Figure 2); the others are mathematically related to the first three. The equilibrium between the protein monomer (P) and dimer (P_2) is

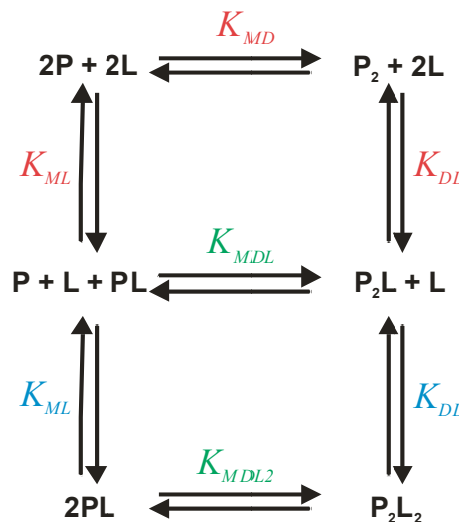


Figure 2. Thermodynamic Model of Coupled Equilibria. Ligand binding by monomeric and dimeric protein (K_{ML} and K_{DL} , respectively) is coupled to protein dimerization (K_{MD} , K_{MDL} , and K_{MDL2}).

characterized by the equilibrium dissociation constant K_{MD} ,

$$K_{MD} = \frac{[P]^2}{[P_2]} \quad (1)$$

The monomer can bind to a single molecule of ligand (L) with equilibrium dissociation constant K_{ML} , defined as:

$$K_{ML} = \frac{[P][L]}{[PL]} \quad (2)$$

whereas the dimer is assumed to bind independently to two molecules of ligand with equilibrium dissociation constant K_{DL} , defined as:

$$K_{DL} = \frac{[P_2][L]^2}{[P_2L_2]} = \frac{[P_2L][L]}{[P_2L_2]} \quad (3)$$

The two additional equilibrium dissociation constants in the model, which characterize heterodimerization of free and ligand-bound monomers (K_{MDL}) and homodimerization of the ligand-bound monomer (K_{MDL2}), are related to the above independent parameters by the relationships:

$$K_{MDL} = \frac{[P][PL]}{[P_2L]} = \frac{K_{MD}K_{DL}}{K_{ML}} \quad (4)$$

and

$$K_{MDL2} = \frac{[PL]^2}{[P_2L_2]} = \frac{K_{MD}K_{DL}^2}{K_{ML}^2} \quad (5)$$

The influence of protein dimerization on ligand binding is represented by the cooperativity factor, c , defined as:

$$c = \frac{K_{DL}}{K_{ML}} = \frac{K_{MDL}}{K_{MD}} = \frac{K_{MDL2}}{K_{MDL}} \quad (6)$$

We aimed to determine each of the equilibrium constants and the cooperativity in the thermodynamic model from the three experimental observables described above and the total concentrations of protein (held constant) and ligand (varied) in a series of samples. The experimental observables are related to the concentrations of species in the thermodynamic model by the following relationships:

$$m = m_{\max} \frac{[PL]}{[P] + [PL]} \quad (7)$$

$$d = d_{\max} \frac{[P_2L] + 2[P_2L_2]}{2[P_2] + 2[P_2L] + 2[P_2L_2]} \quad (8)$$

$$r_{MD} = \frac{[P] + [PL]}{2[P_2] + 2[P_2L] + 2[P_2L_2]} \quad (9)$$

in which m_{\max} and d_{\max} represent the maximum changes in monomer and dimer chemical shifts, respectively, upon ligand binding. Similarly, the total concentrations of protein (P_i) and ligand (L_i) used in the experiment can be expressed as:

$$[P_t] = [P] + [PL] + 2[P_2] + 2[P_2L] + 2[P_2L_2] \quad (10)$$

and

$$[L_t] = [L] + [PL] + [P_2L] + 2[P_2L_2] \quad (11)$$

It is not possible to express the experimental observables explicitly in terms of the thermodynamic parameters. However, the relationships between these parameters can be determined using the iterative algorithm presented in the Supporting Information (Figure S2). To illustrate these relationships, we have simulated the dependence of the experimental observables on ligand concentration for a constant protein concentration (50 μM) and various combinations of equilibrium dissociation constants (Fig. 3). As expected intuitively, variation of the dimerization equilibrium constant (K_{MD} , Fig. 3a) influences the relative intensities of monomer and dimer peaks (r_{MD}) but has no effect on the positions of the two peaks (expressed as m/m_{\max} and d/d_{\max} , respectively). However, as anticipated for a coupled equilibrium system, variation of K_{ML} (Fig. 3b) influences not only the position of the monomer peak (m/m_{\max}) but also the position of the dimer peak (d/d_{\max}) and the relative peak intensities (r_{MD}). Similarly, variation of K_{DL} (Fig. 3c) influences all three observable parameters. Consequently, in order to determine the values of K_{MD} , K_{ML} and K_{DL} (and therefore the

cooperativity factor c) it is necessary to globally fit all three experimental parameters to the thermodynamic model.

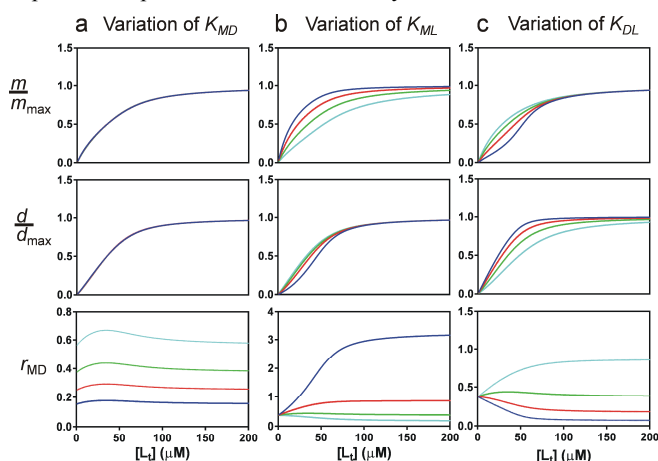


Figure 3. Simulation of NMR Parameters. Values of monomer and dimer peak positions (m/m_{\max} and d/d_{\max}) and the ratio of peak intensities (r_{MD}) were simulated for several different values of (a) K_{MD} , (b) K_{ML} and (c) K_{DL} (2 μM , blue; 5 μM , red; 10 μM , green; and 20 μM , cyan). In each case the other equilibrium constants were set to 10 μM .

Determination of Thermodynamic Parameters from NMR Data

We have used the above thermodynamic model (Fig. 2) to determine the influence of MCP-1 dimerization on binding to CCR2 sulfopeptides. ^{15}N -HSQC spectra were recorded for samples of 50 μM ^{15}N -labeled MCP-1 alone and in the presence of each of the two receptor peptides 1 and 2 at concentrations of 10, 20, 35, 50, 80 and 150 μM . Spectra were analyzed to yield average values and estimated standard errors of m , d and r_{MD} for the five residues for which both monomer and dimer resonances were resolved across the full range of peptide concentrations used (K19, L25, I42, F43 and C52). Finally, for each peptide the experimental observables were fit to the coupled thermodynamic model, using computational optimization and Monte Carlo simulations, to yield optimal values and standard errors for the independent equilibrium constants and the cooperativity factor.

The globally fitted data are presented in Fig. 4 and the resulting equilibrium constants and cooperativity values are listed in Table 1. Overall there is excellent agreement between the fitted curves and experimental data points. For comparison, we have also fit the binding data for the monomer and dimer peaks independently to a simple 1:1 equilibrium model (Conventional Fits, Table 1 and Figure S3). Although the simple model is not strictly valid for a coupled system, this conventional approach yields K_D values in reasonable agreement with those obtained from the global fitting approach. However, because the conventional K_D determinations are independent for monomer and dimer species, the calculated cooperativity is relatively poorly defined (14-21% error). In contrast, for the global fitting approach, there is a strong correlation between the K_{ML} and K_{DL} values determined for the many Monte-Carlo simulations (Fig. 5). Consequently, the cooperativity value (defined as the ratio of these two equilibrium constants; eqn (6)) is

determined with substantially higher precision by the global fitting approach (error values <5%; Fig. 5, Table 1). Importantly, the global fitting approach clearly shows that cooperativity is higher for sulfopeptide **2** than for sulfopeptide **1**, suggesting that the interactions of the Tyr-28 sulfate group weaken MCP-1 dimerization.

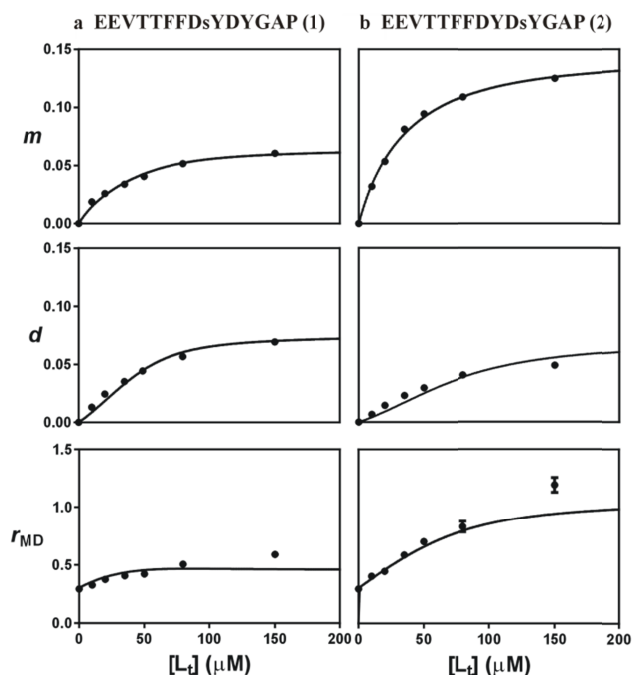


Figure 4. Experimental NMR Data Fitted to the Coupled Thermodynamic Model. Shown are values of monomer and dimer peak shifts (m and d) and the ratio of peak intensities (r_{MD}) determined for MCP-1 in the presence of increasing concentrations of CCR2-derived sulfopeptides (**a**) **1** and (**b**) **2**. Experimental data are the averages for the 5 NH groups for which both monomer and dimer peaks were observable across the full range of peptide concentrations used. Error bars (representing standard errors) are plotted but are smaller than the data points in many cases. Solid lines show the best fits of the experimental data to the coupled thermodynamic model in Fig. 2.

Peptide	K_{ML} (μM)	K_{DL} (μM)	c
Conventional Fits ^a			
1	27.8 ± 5.4	28.1 ± 2.1	1.01 ± 0.21
2	20.1 ± 1.2	46.1 ± 6.2	2.29 ± 0.33
Global Fits to Coupled Thermodynamic Model ^b			
1	10.0 ± 1.7	14.4 ± 2.5	1.42 ± 0.04
2	15.5 ± 3.3	43.4 ± 10.5	2.80 ± 0.14

Table 1 Fitted Equilibrium Binding Constants and Cooperativity Values for Binding of MCP-1 to CCR2-derived Sulfopeptides **1** and **2**. ^aConventional fits were performed independently for monomer and dimer data using a simple 1:1 binding model with the concentration of the monomer or dimer species assumed to be halfway between the two extreme concentrations deduced from the peak intensities in Figure 4. ^bGlobal fits were performed using the coupled thermodynamic model in Figure 2.

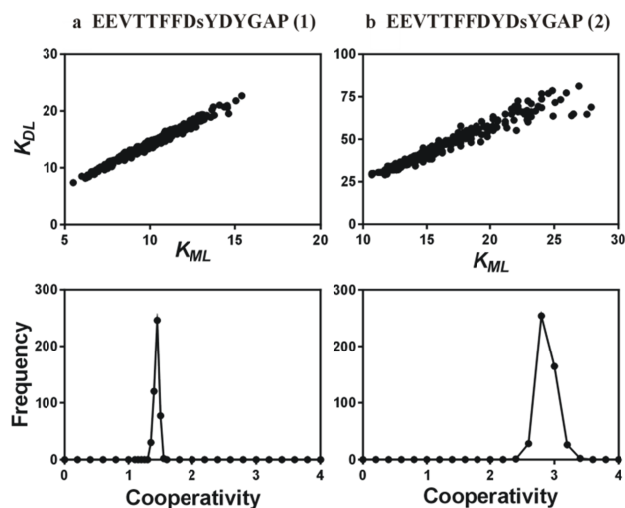


Figure 5. Distributions of Equilibrium Binding Constants and Cooperativity Values. Top panels show the fitted values of K_{ML} and K_{DL} obtained in each of the 475 best Monte-Carlo simulations for binding of MCP-1 to (**a**) **1** and (**b**) **2**. Lower panels show the corresponding distributions of cooperativity (c) values. Methods for Monte-Carlo simulations are described in the Supporting Information.

It is noteworthy that the cooperativity values observed here are very low in comparison to classical cooperative binding proteins or allosteric enzymes. Therefore, while binding of MCP-1 to the sulfated N-terminus of CCR2 does appear to weakly induce dimer dissociation, the biological consequences of this thermodynamic coupling are expected to be very subtle. It remains possible, albeit speculative, that subsequent interactions of MCP-1 with other regions of CCR2 further select for the monomeric, active form of the chemokine ligand.

A possible complicating factor in the method presented here is that the intensities of monomer and dimer resonances could be influenced not only by the populations of the two species but also by differences in their relaxation properties giving rise to differences in line shapes. This could be particularly significant if one species were undergoing a chemical exchange process not present in the other species or if one species were undergoing selective aggregation. Such relaxation effects would not influence r_{MD} values determined from peak integrals (rather than peak heights), but, as in the current application, accurate measurement of peak integrals is often impractical due to low signal-to-noise ratios or partial overlap of resonances. Line broadening effects could be further investigated by direct measurement of transverse relaxation rates for monomer and dimer resonances as a function of ligand concentration; in theory, it would then be possible to correct the r_{MD} values to compensate for line broadening.

In the current study, the dimer resonance for Leu-25 appears to be selectively broadened in the final titration point with sulfopeptide **2** (Fig. 1b), although for other residues both monomer and dimer resonances were broadened in the final titration point (Figure S1). These results suggest some sample aggregation may have occurred towards the end of the titration, possibly influencing

the dimer more than the monomer and therefore contributing to the poorer fit of r_{MD} data for the later titration points of sulfopeptide **2** (Fig. 4). Nevertheless, such line broadening effects are not expected to influence the peak positions, which are the primary determinants of binding equilibrium constants (K_{ML} and K_{DL}) and therefore the cooperativity values. Thus, the observed line broadening does not change the overall conclusion that cooperativity is higher for sulfopeptide **2** than sulfopeptide **1**.

Potential Applicability to Other Systems

The method presented herein is theoretically applicable to any system involving two coupled equilibrium processes in which one process is fast and the other is slow on the NMR chemical shift time scale. This might include proteins whose dimerization is coupled to binding of oligosaccharides, small molecules, or metal ions, as reported previously.²⁵⁻²⁷ Alternatively the slow process of proline isomerization within proteins may be coupled to binding of partner proteins.²⁸⁻²⁹ For example, Breheny *et al.* have studied the slow equilibrium between proline *cis* and *trans* isomers within the Src homology 2 (SH2) domain of interleukin-2 tyrosine kinase (Itk).²⁹ The two isomers have similar populations in the unbound domain but binding to a phosphotyrosine-containing peptide biases the equilibrium towards the *trans* isomer whereas binding to the Itk SH3 domain biases the equilibrium towards the *cis* isomer. More broadly, one can envisage other slow equilibria, such as binding to a slowly-dissociating ligand, alteration of interdomain contacts or protein folding, being thermodynamically coupled to fast equilibria, such as binding to fast-dissociating ligands or side chain protonation/deprotonation.

In addition to the requirement that the two exchange processes occur with substantially different kinetics, several other factors may limit the practical application of the approach described here. First, the total concentration of protein used must be close enough to the K_{MD} value to yield observable populations (at least ~10%) of each species (monomer and dimer). Second, as with most binding experiments, the total protein concentration must be less than or similar to both the K_{ML} and K_{DL} values, allowing observation of non-linear chemical shift changes upon addition of ligand. Finally, the signal-to-noise ratios of all peaks must be high enough, and the line widths must be narrow enough, to allow quantification of peak positions and intensities for all species across the full range of ligand concentrations used. With current NMR technology, this method is therefore limited to the K_{MD} , K_{ML} and K_{DL} values in the micromolar to millimolar range. However, future technological innovations may allow higher affinity equilibria to also be investigated using this approach.

Conclusions

In summary, we have presented a general framework for analysis of 2D NMR spectra to evaluate the cooperativity of ligand binding and protein dimerization in coupled systems. This method is applicable to any system in which dimerization is slow and ligand binding is fast on the NMR chemical shift time scale and in which both

monomer and dimer resonances are resolvable in a practical range of protein and ligand concentrations. We have applied this approach to a system in which the thermodynamics are well described by the simple thermodynamic model presented in Fig. 2. However, the same strategy could potentially be used for more sophisticated models involving, for example, higher order oligomers or non-independent binding sites on oligomeric proteins. The approach presented here extends the array of NMR-based methods for characterisation of chemical and binding equilibria.

Acknowledgements

This work was supported by Australian Research Council grants DP1094884 and DP130101984 (to R.J.P. and M.J.S.) and LE0989504 (to M.J.S.).

Notes and references

^aDepartment of Biochemistry and Molecular Biology, Monash University, Clayton, VIC 3800, Australia

^bSchool of Chemistry, Monash University, Clayton, Victoria 3800, Australia

^cSchool of Chemistry, The University of Sydney, Sydney, New South Wales 2006, Australia

*Corresponding author: martin.stone@monash.edu

Electronic Supplementary Information (ESI) available: Experimental, data analysis and fitting methods and the iterative computational algorithm used for simulation of NMR parameters. See DOI: 10.1039/b000000x/

- 1 N. J. Marianayagam, M. Sunde and J. M. Matthews, *TIBS*, 2004, **29**, 618.
- 2 J. M. Matthews (Ed), *Advances in Experimental Medicine and Biology*, Protein Dimerization and Oligomerization in Biology, Springer Berlin, Germany, 2012, **747**.
- 3 A. Levitzki and J. Schlessinger, *Biochemistry*, 1974, **13**, 5214.
- 4 A. V. Hill, *J. Physiol. (Lond.)*, 1910, **40**, iv.
- 5 L. W. Nichols and D. J. Winzor, *Biochemistry*, 1976, **15**, 3015.
- 6 G. Scatchard and N. Y. Ann, *Acad. Sci.*, 1949, **51**, 93.
- 7 C. Freiden, *J. Biol. Chem.*, 1967, **242**, 4045.
- 8 G. K. Wolfer, J. L. Neil, W. Barton Rippon, *J. Prot. Chem.*, 1987, **6**, 441.
- 9 K. Julenius, J. Robblee, E. Thulin, B. E. Finn, R. Fairman, S. Linse, *Proteins Struct. Func. Genet.*, 2002, **47**, 323.
- 10 B. Moser, M. Wolf, P. Loetscher, *TIBS*, 2004, **25**, 75.
- 11 D. J. Scholten, M. Canals, D. Maussang, L. Roumen, M. J. Smit, M. Wijtman, C. de Graaf, H. F. Vischer, R. Leurs, *Brit. J. Pharmacol.*, 2012, **165**, 1617.
- 12 J. P. Ludeman and M. J. Stone, *Brit. J. Pharmacol.*, 2013, **171**, 1167.
- 13 J. H. Y. Tan, J. P. Ludeman, J. Wedderburn, M. Canals, P. Hall, S. J. Butler, D. Taleski, A. Christopolous, M. J. Hickey,

- R. J. Payne, and M. J. Stone, *J. Biol. Chem.*, 2013, **288**, 10024.
- 14 C. D. Paavola, S. Hemmerich, D. Grunberger, I. Polsky, A. Blom, R. Freedman, M. Mulkins, S. Bhakta, D. McCarly, L. Wiesent, B. Wong, K. Jarnagin and T. M. Handel, *J. Biol. Chem.*, 1998, **273**, 33157.
- 15 T. M. Handel and P. J. Domaille, *Biochemistry*, 1996, **35**, 6569.
- 16 J. F. Paolini, D. Willard, T. Consler, M. Luther, M. S. Krangel, *J. Immunol.*, 1994, **153**, 2704.
- 17 E. J. Fernandez, E. Lolis, *Annu. Rev. Pharmacol. Toxicol.*, 2002, **42**, 469.
- 18 J. H. Y. Tan, M. Canals, J. P. Ludeman, J. Wedderburn, C. Boston, S. J. Butler, A. M. Carrick, T. R. Parody, D. Taleski, A. Christopolous, R. J. Payne and M. J. Stone, *J. Biol. Chem.*, 2012, **287**, 14692.
- 19 H. Jin, X. Shen, B. R. Bagget, X. Kong, P. J. LiWang, *J. Biol. Chem.*, 2007, **282**, 27976.
- 20 C. T. Veldkamp, C. Seibert, F. C. Peterson, N. B. De la Cruz, J. C. Haugner III, H. Basnet, T. Sakmar, B. F. Volkman, *Sci. Signal.*, 2008, **1**, ra4.
- 21 M. W. Nasser, S. K. Raghuwanshi, D. J. Grant, V. R. Jala, K. Rajarathnam, R. M. Richardson, *J. Immunol.*, 2009, **183**, 3425.
- 22 L. Drury, J. J. Ziarek, S. Gravel, C. T. Veldkamp, T. Takekoshi, S. T. Hwang, N. Heveker, B. F. Volkman, M. B. Dwinell, *PNAS*, 2011, **108**, 17655.
- 23 P. Gangavarapu, L. Rajagopalan, D. Kolli, A. Guerrero-Plata, R. P. Garofalo, K. Rajarathnam, *J. Leukoc. Biol.*, 2012, **91**, 259.
- 24 A. Ravindran, K. V. Sawant, J. Sarmiento, J. Navarro, K. Rajarathnam, *J. Biol. Chem.*, 2013, **288**, 12244.
- 25 J. Flint, D. Nurizzo, S.E. Harding, E. Longman, G.J. Davies, H.J. Gilbert, D.N. Bolam, *J. Mol. Biol.*, 2004, **337**, 417.
- 26 C.T. Rollins, V.M. Rivera, D.N. Woolfson, T. Keenan, M Hatada, S.E. Adams, L.J. Andrade, D. Yaeger, M.R. van Schravendijk, D.A. Holt, M. Gilman, T. Clackson, *PNAS.*, 2000, **97**, 7096.
- 27 K. Julenius, J. Robblee, E. Thulin, B.E. Finn, R. Fairman, S. Linse, *Proteins: Struct Func Gen*, 2002, **47**, 323.
- 28 C.M. Santiveri, J.M. Perez-Canadillas, M.K. Vadivelu, M.D. Allen, T.J. Rutherford, N.A. Watkins, M. Bycroft, *J. Biol. Chem.*, 2004, **279**, 34963.
- 29 P.J. Breheny, A. Laederach, D.B. Fulton, A.H. Andreotti, *J. Am. Chem. Soc.*, 2003, **125**, 15706.

Table of Contents Graphic

